

Copyright
by
Wenbin Ouyang
2013

**The Thesis Committee for Wenbin Ouyang
Certifies that this is the approved version of the following thesis:**

Evaluating Fabric Pilling/Wrinkling Appearance Using 3D Images

**APPROVED BY
SUPERVISING COMMITTEE:**

Supervisor:

BugaoXu

Julia A. (Ann) Reed

Evaluating Fabric Pilling/Wrinkling Appearance Using 3D Images

by

Wenbin Ouyang, B.E.; M.E.

Thesis

Presented to the Faculty of the Graduate School of

The University of Texas at Austin

in Partial Fulfillment

of the Requirements

for the Degree of

Master of Science in Textile and Apparel Technology

The University of Texas at Austin

December 2013

Abstract

Evaluating Fabric Pilling/Wrinkling Appearance Using 3D Images

Wenbin Ouyang, M.S.T.A.T.

The University of Texas at Austin, 2013

Supervisor: Bugao Xu

Fabric appearance is usually the highest priority consideration for consumers. Pilling and wrinkling are two major factors which cause the fabric to have a worse appearance after a certain service period. In order to prevent more piling and wrinkling, a fabric pilling and wrinkling severity evaluation is very important. Traditional visual examination needs at least three trained experts to judge each sample, which is both subjective and time-consuming. Objective, high efficiency, and automatic pilling and wrinkling evaluation based on computer processing techniques are now being developed quickly.

In this study, an integrated fabric pilling and wrinkling measurement system based on stereovision was developed. The hardware part of the system consists of a pair of consumer high resolution cameras and a mounting stage, which is affordable and portable in comparison with other 3D imaging systems. A novel pilling detection

algorithm focusing on 3D image local information was proposed to extract three pilling features including pilling density, pilling average height, and pilling average size. The logistic regression classifier was applied for pilling severity classification because it showed a good accuracy with 80% on the 120 3D pilling images.

A fast wrinkle detection algorithm with leveled 3D fabric surface was developed to measure wrinkle density, hardness, tip-angle, and roughness. According to these four wrinkling features, 180 3D wrinkling images were tested by the logistic regression classifier with an overall 74.4% accuracy in comparison with visual judging results.

Both pilling and wrinkling results obtained from the proposed automatic 3D fabric pilling and wrinkling severity evaluation system were consistent with the subjective visual evaluation results. The system is ready for practical use.

Table of Contents

List of Tables	viii
List of Figures	ix
Chapter 1: Introduction.....	1
1.1 Motivation and Goals.....	1
1.2 Background of Fabric Appearance	2
1.2.1 Fabric Pilling.....	2
1.2.2 Fabric Wrinkling	3
1.3 Methods for Fabric Pilling/Wrinkling Appearance Measurement	4
1.3.1 Traditional Evaluation Methods.....	4
1.3.2 2D Image Processing Evaluation Methods.....	7
1.4 3D Measurement for Fabric Pilling/Wrinkling Appearance	8
1.5 Structures of the Thesis	10
Chapter 2: Framework of Pilling/Wrinkling Appearance Evaluation System.....	12
2.1 Stereo Vision System	12
2.2 System Setup	14
2.3 Camera Calibration	14
Chapter 3: Measurement of Fabric Pilling.....	16
3.1 Introduction	16
3.2 Pilling Measurement	17
3.2.1 Pilling Seed Searching.....	17
3.2.2 Pilling Seed Region Growing	20
3.2.3 Pilling Feature Determination.....	22
Chapter 4: Measurement of Fabric Wrinkling	23
4.1 Introduction	23
4.2 Wrinkle Measurement.....	23

4.2.1 Fabric Surface Leveling.....	23
4.2.2 Wrinkle Detection	26
4.2.3 Wrinkle Feature Extraction.....	30
Chapter 5: Experimental Results Analysis	33
5.1 Sample Preparation	33
5.1.1 Pilling Sample Preparation	33
5.1.2 Wrinkle Sample Preparation.....	33
5.2 Pilling Experiments.....	34
5.3 Wrinkle Experiments	41
Chapter 6: Conclusions and Future Work.....	45
6.1 Summary of the Thesis.....	45
6.2 Suggested Future Work.....	46
Bibliography	48

List of Tables

Table 5.1 Illustration of surface projection onto the base plane.	34
Table 5.2 3D and manual measurements of pilling density (D), height (H) and area (A). 36	
Table 5.3 Regression analysis between pilling grades and pilling features.	38
Table 5.4 Classification by the logistic regression classifier.	39
Table 5.5 Classification by the naïve Bayes classifier.	39
Table 5.6 Classification by the linear SVM.	39
Table 5.7 3D images and pilling densities of three different samples.	40
Table 5.8 Wrinkle roughness raw data.	42
Table 5.9 Normalized wrinkle roughness data.	42
Table 5.10 Importance of components.	43
Table 5.11 The logistic regression classification results of 180 3D wrinkling images.	44

List of Figures

Figure 1.1 The same fabric after different laundry cycles: (a) 25, (b) 50, (c) 75, and (d) 100.....	3
Figure 1.2 ASTM standard replicas for pilling assessment.....	5
Figure 1.3 AATCC standard replicas for wrinkling assessment.....	6
Figure 2.1 Stereovision system setup.....	12
Figure 2.2 Principle of stereovision.....	13
Figure 2.3 System calibration pattern.....	15
Figure 3.1 Pilling detection result by overall thresholding method, (a) original 3D image and (b) overestimated pilling areas by direct thresholding.....	16
Figure 3.2 Dune-like pills, (a) semi-sphericity shape and (b) ellipsoidal shape.....	17
Figure 3.3 Pilling seed detection, (a) peak map and (b) pilling seeds.....	18
Figure 3.4 Crossing profiles at a peak, (a) dune shape, (b) horizontal profile, and (c) vertical profile.....	19
Figure 3.5 Map of detected pilling areas from Figure 3.1a.....	21
Figure 3.6 Illustration of surface projection onto the base plane.....	22
Figure 4.1 3D image surface leveling, (a) raw 3D image data, (b) NURBS surface (elevation plane), and (c) Leveled fabric surface.....	26
Figure 4.2 Wrinkle direction chart.....	26
Figure 4.3 Close-view of a part of a row in 3D image.....	28
Figure 4.4 Wrinkle detection intermediate result, (a) raw 3D image and (b) intermediate result.....	28
Figure 4.5 Wrinkle detection result.....	30
Figure 4.6 Close-up of wrinkle area showing the transverse profile <i>AB</i> and <i>CD</i>	31
Figure 5.1 Pilling density measurements.....	37
Figure 5.2 Distribution of one dimensional wrinkle roughness feature vector by PCA.....	43

Chapter 1: Introduction

1.1 MOTIVATION AND GOALS

As with any garment, after a certain service period, its aesthetic appearance will deteriorate. Wrinkles and pilling are the two major factors in a garment's worn or aged appearance. Wrinkles are easily formed by folding and pressing during ordinary wearing and washing. Long time abrasion and tumbling will generate pilling. For garments, pilling may easily appear at elbow part and backside. In order to extend garments serving time, easy-care garments conception was proposed and now it becomes more and more popular. Fabrics for easy-care garments mean that fabrics were processed wrinkling-resistant and pilling-resistant before finishing. The severity of fabric wrinkling and pilling is routinely examined for quality assurance. Therefore, textile manufacturers and researchers put lots of efforts on fabric wrinkling and pilling evaluation. Wrinkles and pilling detections are taken as a kind of property investigation of target fabric, which is significant in the research of fabric material development and application.

Although some quantitative methods including 2D digital image processing technology [1-8], 2D infrared imaging system [9], and 3D imaging technology [10-12] have been developed, visual examination for wrinkling and pilling is still the only method that is standardized and widely accepted in the textile industry; still, this conventional method is both subjective and time-consuming. The major flaw of 2D image processing is that the measurement accuracy highly depends on fabric colors or texture patterns. Comparingly, the 2D infrared imaging system has no influence on fabric color and texture, but a lower resolution and redundant noise does not allow the system to detect pilling. 3D imaging technology has a good potential, but up to now, there is no integrated

system that can measure both wrinkling and pilling, while providing a quantitative understanding of the replicas used for visual examination.

The principle goal of this study is to design an integrated fabric pilling and wrinkling appearance evaluation system, and to present a physical meaning— length, density, etc. — of the visual evaluation replicas for both wrinkling and pilling.

1.2 BACKGROUND OF FABRIC APPEARANCE

Aesthetic appeal of a garment includes its appearance, its hand, and even its scent. Fabric appearance includes several aspects, such as: wrinkling, stiffness, pilling, colorfastness, dimensional stability, stain removal, water repellency, etc. When purchasing, most consumers regard aesthetic appearance as a priority, because their first impression of the garment is based on visual aspects. Usually, if a garment has an easy care label such as no-wrinkle or pilling-resistant, it will be more attractive to most consumers.

1.2.1 Fabric Pilling

Pilling occurs when several balls form on the surface of a fabric due to abrasion, longevity, and give an undesirable appearance. Short fibers pill more due to their loose ends protruding out of yarns. Smooth fiber materials, like nylon, however, resist pilling more readily as opposed to rougher ones, like wool. Higher strength fibers hold pilling on the surface more securely and take on obvious pilling appearance. Higher linear density fabrics with coarser and heavier yarns pill much easier. Higher thread count structures, found in plain weave fabrics, could pill less, a factor attributing to their compactness. Fabrics cannot avoid the generating of pilling, and the quantity of pilling will only

increase with a longer service period. Figure 1.1 lists pilling effects after different laundry cycles from 25 to 100 of the same fabric.

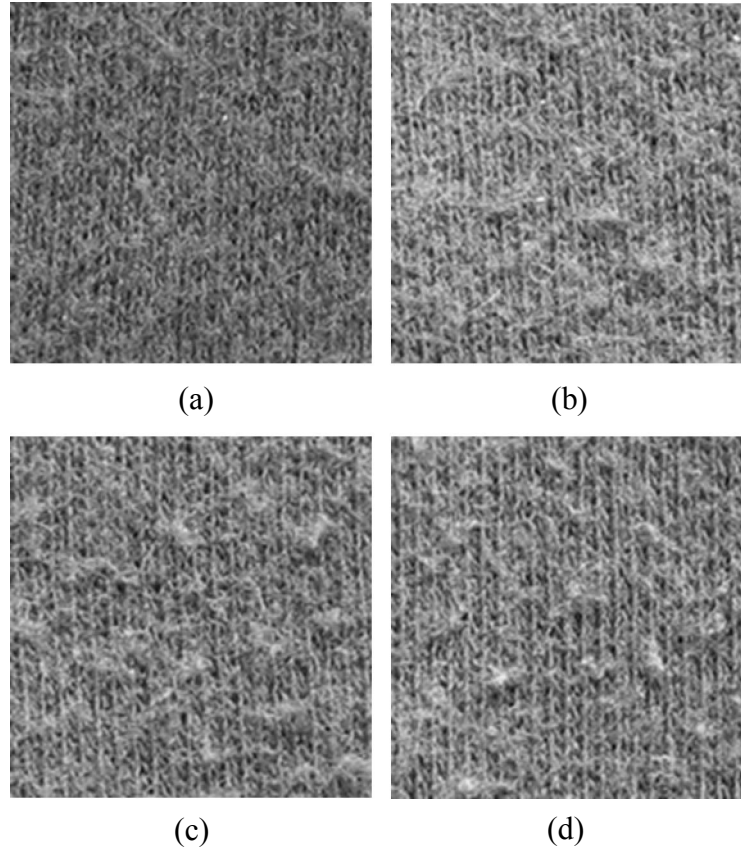


Figure 1.1 The same fabric after different laundry cycles: (a) 25, (b) 50, (c) 75, and (d) 100.

1.2.2 Fabric Wrinkling

Wrinkling, a kind of residue bending deformation that appears on the surface of the fabric, can be caused by the motions of wearers, folding, and washing. Wrinkling is a physical phenomenon, and it is influenced by several intrinsic properties of fabrics. Short fibers produce more obvious wrinkles than longer fibers because of their easy displacement and permanent deformation maintenance. Fibers with round cross-sectional geometry resist bending stronger than other types of fiber shapes. Medium twisted fabrics have little chance to be displaced compared with low twisted and high twisted ones.

Lower thread count fabrics own higher yarn mobility and resist bending easily. Certainly, a fiber's composition also plays a crucial role in wrinkling production. Wool ranks in first place for higher wrinkling resistance, and the next two are silk and nylon when compared with cotton and flax.

1.3 METHODS FOR FABRIC PILLING/WRINKLING APPEARANCE MEASUREMENT

1.3.1 Traditional Evaluation Methods

The traditional wrinkling and pilling measurements are both based on the visual examination which compares fabric samples with different levels of standard replicas. Pilling conditions are quantified by a standard set of photographic pilling standards supplied by ASTM, as seen in Figure 1.2. Five grades from most severe pilling, grade 1, to no pilling, grade 5, were defined to describe fabric pilling condition.

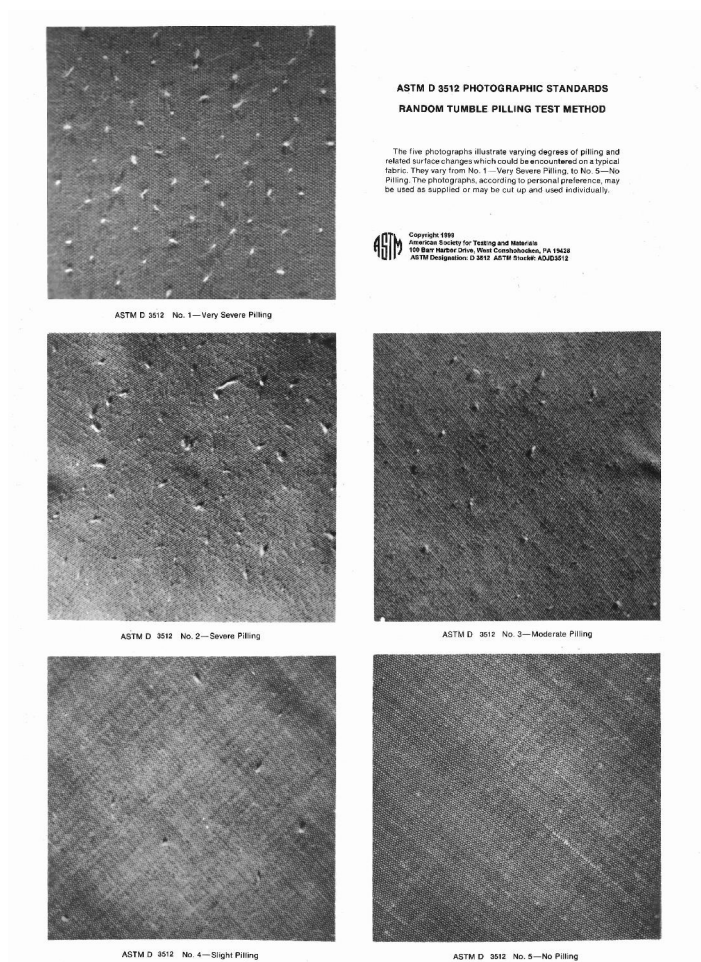


Figure 1.2 ASTM standard replicas for pilling assessment.

In most cases, wrinkling results are measured with 3-dimensional reference standards from grade 1 to grade 5, as seen in Figure 1.3. This AATCC Test Method 124 firstly defined five wrinkling grades from severe wrinkling, SA-1, to very smooth, SA-5, as a fabric wrinkling measurement. SA-3.5 was added to the standard to describe a fairly smooth, non-pressed appearance [13].

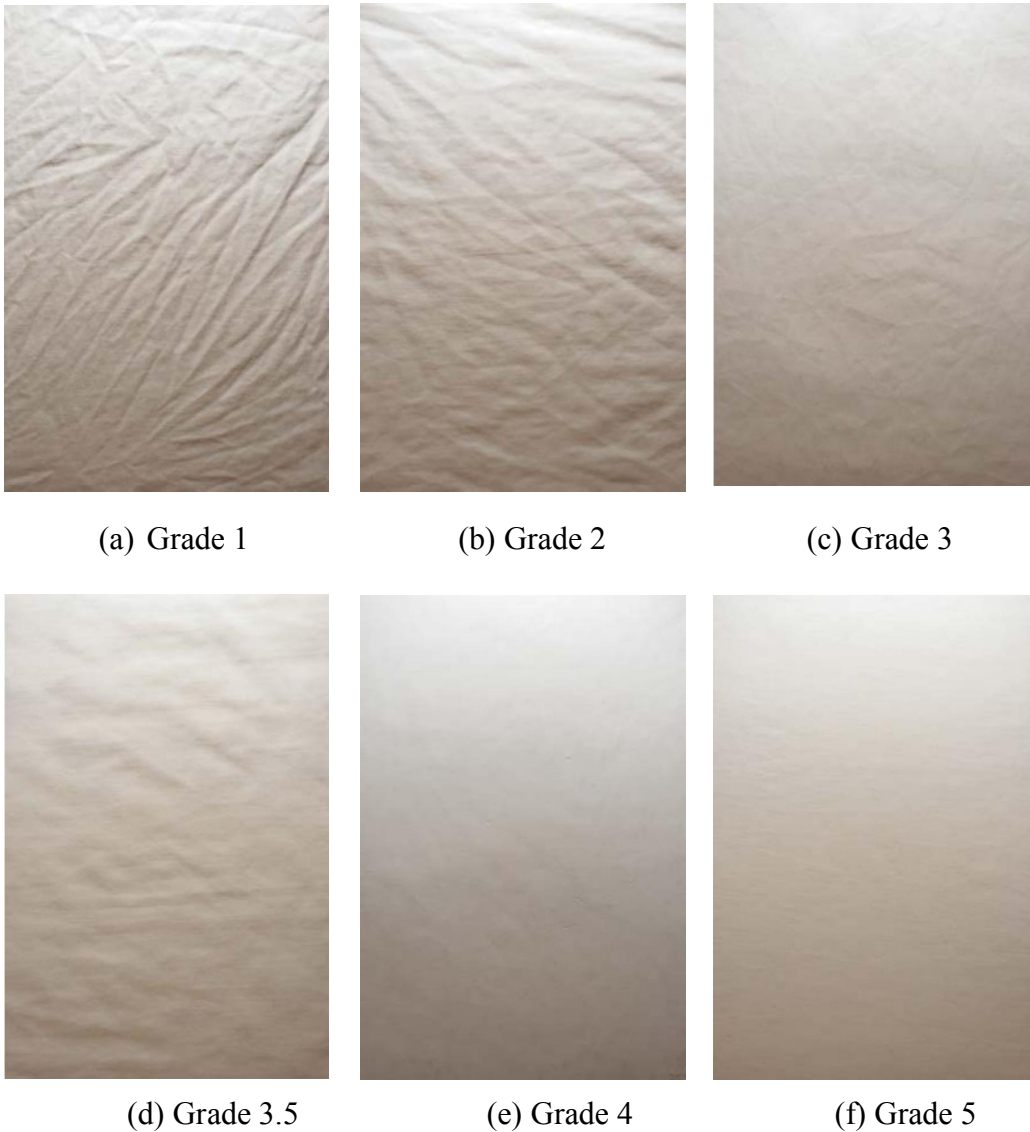


Figure 1.3 AATCC standard replicas for wrinkling assessment.

Visual examination method is mostly traditional, and being widely used in the textile related laboratories and industries. For this method, at least three trained observers should independently judge specimens. Several issues in this method include being time-consuming, subjective, and unreliable. Even for a given fabric sample, it is impossible to

get identical opinion across different raters. Thus, the accuracy of traditional evaluation methods limits its further adoption.

1.3.2 2D Image Processing Evaluation Methods

In order to overcome the shortcomings of traditional evaluation methods, algorithms based on 2D image processing methods were developed, starting with 1990s [1-8]. Xu et al. and Na et al. relied on computer image analysis to measure the wrinkles from surface ratio and shade ratio parameters, which were highly correlated with different levels of AATCC wrinkle recovery replicas [1, 2]. Choi et al. applied 2D-FFT (Fast Fourier Transform) to the fabric surface [4]. FFT is a kind of signal procession, which transformed wrinkle data into small circles with different types and numbers. Through the analysis of such transformed circles, different smoothness levels can be determined. Although the algorithm developed by Choi et al. [4] was a big breakthrough in the field of wrinkle measurements at that time, gray-scaled input images were strongly sensitive to light sources and image noises, which limited the performance of such method. Zaouali et al. proposed another image analysis algorithm from several wrinkle descriptors, such as wrinkle density, profile, sharpness, randomness, overall appearance, and fractal dimension [3], which were suggested by Johnson [14]. The complexity and time consumption of this algorithm were high. Furthermore, it cannot process large pieces of fabric or printed fabrics.

Digital image analyzing for pilling measurements have been proposed in [5-8]. Xu applied the Fast Fourier Transform to remove weave texture information from an image, and a template-matching scheme to locate pilling areas [5]. Torreset et al. took advantage of spatial and frequency domain operations to calculate pilling areas [6]. Wagner correlated pilling area with axes length ratio (pill major axis breadth / pill major

axis length) to eliminate unwanted textural effects highlighted by an oblique lighting [7]. Xin et al. carried on the idea of obtaining a pill threshold from a trained pill template which uses a 2D Gaussian fit method on a batch of pill images [8].

1.4 3D MEASUREMENT FOR FABRIC PILLING/WRINKLING APPEARANCE

Because 2D imaging processing method had obvious defects on colored or printed fabric, 3D fabric surface reconstruction methods were proposed. The 3D measurement systems, called “color-blind” systems, are independent of changes of sample colors and therefore can improve the reliability of detecting surface features in the 3D space [15, 16]. With the introduction of the laser probe, whose resolution has the order of micron, more and more fabric image analysis were processed under the assistance of such technology [17] to ensure highly precise results. Su and Xu composed laser triangulation formed by projectors, cameras and fabrics samples, and image processing technologies together, which used a neural network to classify the wrinkle respecting to the visual replicas [12]. Laser line projector worked onto the fabric sample that was placed on a rotating stage, and the computer received the images captured by CCD camera above the sample. Because of the sample rotating duration, the whole data acquisition time of this method was longer. Compared with laser probe, CCD camera owns higher visual image density and performs the same visual effect as human observations. This system advanced wrinkle measurement because of its high degree of automation and reliability. However, its high accuracy of mechanical requirements caused lower efficiency and higher cost. The limitation of the system was only orientated to measure wrinkling, making the system limited in its acceptance. Other 3D systems include laser line-scanning system for fabric imaging developed by Abidi [18], and a grid-line projection

technique for fabric 3D shaped image by Kang et al. [11]. These 3D wrinkling measurement systems' efficiency and accuracy were restricted.

A laser range sensor based on 3D fabric fuzziness and pilling measurement system was proposed by Xu and Yao [10]. This system with a high scanning resolution about 10 micrometers was able to detect detailed information such as pilling and fuzziness on the fabric. In order to achieve a higher resolution, the system would be very time consuming since the laser point needs to move in both x and y directions. Limited scanning area resulted a specimen not fully been scanned. This was an additional limitation for the system.

Compared to scanning-based 3D sensing technology, stereovision appears to be a more efficient and economical approach for fabric surface reconstruction, because it only requires a pair of images taken by two regular digital cameras [16]. With a proper setup and calibration, a stereovision system can possess high resolutions in x , y and z , and generate a 3D image that shows fine structures on the fabric surface [15]. Data acquiring time is the camera's aperture time with a high efficiency, which is less than 10 micro seconds. This system has no scanning area limitation, which suits different size fabrics.

In this research, we attempted to develop new algorithms for pilling and wrinkling detection and characterization using 3D information of a fabric surface. 3D fabric images are first generated using a stereovision system developed in the prior study. Based on the depth information available in the 3D image, the pilling detection process starts from the seed-searching at local depth maxima to the region-growing around selected seeds using both depth and distance criteria. The pilling appearance can be characterized by the density, heights and areas of individual pills in the image. The depth information in a 3D

image permits more reliable pilling detections and more comprehensive descriptions of pilling features than in a 2D image.

The wrinkling detection procedure directly used the depth information in the 3D image. Each 3D wrinkling image was firstly leveled by B-spline method. After detecting the ridge and valley points in the 3D image, four wrinkling features— density, hardness, tip-angle, and roughness— determine the fabric severity level.

1.5 STRUCTURES OF THE THESIS

This thesis will cover four parts, Chapter 2 to Chapter 6, to report our contribution to the research of both fabric wrinkling and pilling appearance measurement.

Chapter 2 will discuss the “Framework of pilling/wrinkling appearance evaluation system” including the stereovision system setup, principle of stereovision, and camera calibration.

Chapter 3 describes the measurement of fabric pilling using 3D images generated by the stereovision system. In this part, a novel pilling detection algorithm majorly based on the 3D image local information will be discussed. According to a pill’s dune like shape, peak points firstly will be found in 3D images. Then, each found peak point will be set as a seed, and a local seed growing method will be applied to measure the pilling size. Three pilling features are extracted: pilling density, as overall pilling information, is the first measurand. Pilling average height and average base plane area are two additional measurands, which describe the fabric pilling severity in more details.

Chapter 4 presents a new and fast algorithm for fabric wrinkling detection. Fabric surface leveling is firstly used to prepare a leveled 3D image for further wrinkle detection. With a leveled surface, wrinkle peak or valley points can be fast detected in

certain ranges. Wrinkling density, sharpness, tip-angle, and roughness are four measured features in this system.

In order to give a quantitative meaning for pilling and wrinkle replicas, chapter 5 will find a suitable classifier according to both pilling and wrinkle features. 120 3D images generated from 30 pilling fabrics with different fiber contents, weave structures, colors and laundering cycles consist a training set for building the pilling classifier. These 30 pilling fabrics, 6 for each level, have been judged by three independent persons using visual method in advance. As for the wrinkle part, 3D images of 6 wrinkle replicas behave as physical standards for wrinkle severity and provide quantitative data results in building the wrinkle classifier. Then 180 3D images generated from 30 wrinkling-severity-leveled fabrics will be used to verify the validity of the chosen classifier.

Chapter 6 offers a conclusion and future work for this study.

Chapter 2: Framework of Pilling/Wrinkling Appearance Evaluation System

Basically, there are three categories of technologies employed in three-dimensional scanning systems: light-based, laser-based, and stereovision systems. Stereovision system is in the manner similar to human vision effect, and it is the safest and most accurate one among these three categories, which can be applied to wrinkling and pilling detections and evaluations. In this chapter, the basic working principles, system setup, and calibration method of the stereovision system are described.

2.1 STEREO VISION SYSTEM

Stereo-photogrammetric system determines 3D structure of a scene or an object from two or more cameras taken from different positions.

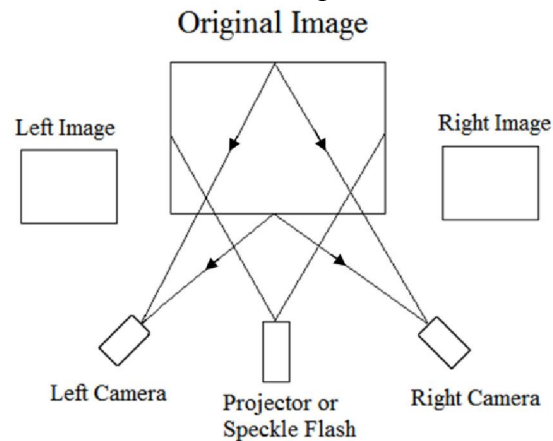


Figure 2.1 Stereovision system setup.

Stereo matching process is a crucial step to find pixels from the camera taken pictures corresponding to the same special point. Matching algorithms for stereovision system can be classified into two categories [19], one is local correspondence methods, and the second is global correspondence methods. Local methods cover the aspects:

block matching [20], gradient methods [21], and feature matching [22]. Global methods involve: dynamic programming [23], intrinsic curves [24], and graph cuts [25]. The purpose of the stereo matching is to figure out the relative displacement between the pictures, which is called disparity. Through the analysis of disparity, depth information from 3D target can be obtained. The basic stereovision based structure is shown in Figure 2.1.

In order to display the principle of stereovision system, Figure 2.1 can be transformed to the form of axes-based structure, as shown in Figure 2.2. Point P is the target point with its position (X, Y, Z) . In a left-sided image taken by the left camera, the position of P can be expressed as (i_l, j_l, f) , and the same to a right-sided image, P is found in the position (i_r, j_r, f) .

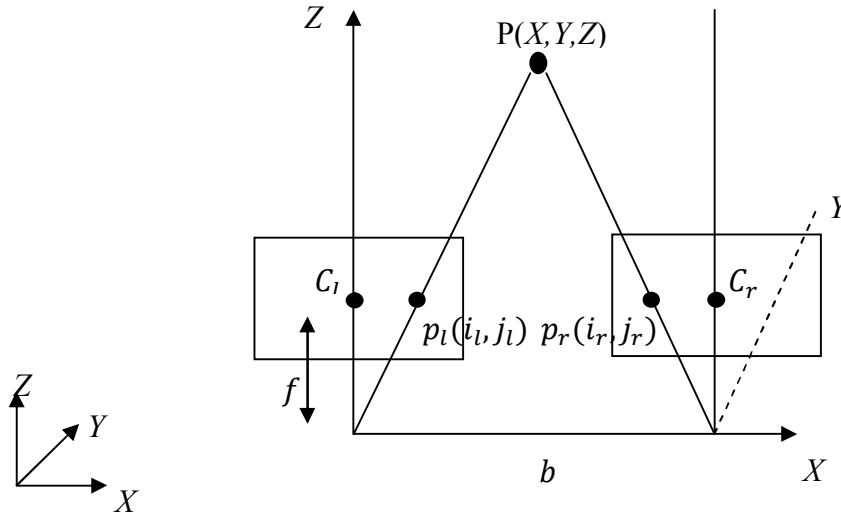


Figure 2.2 Principle of stereovision.

The disparity between left and right images can be expressed as:

$$d = i_l - i_r \quad (2.1)$$

And because of the same distances in Y direction, we have:

$$j_l = j_r \quad (2.2)$$

The magnification coefficient C can be calculated through:

$$C = \frac{b}{a} = \frac{b}{i_l - i_r} \quad (2.3)$$

Finally, the real word position of P can be derived by equation 2.4

$$\begin{bmatrix} X \\ Y \\ Z \end{bmatrix} = C \begin{bmatrix} i_l \\ j_l \\ f \end{bmatrix} = C \begin{bmatrix} i_r + b \\ j_r \\ f \end{bmatrix} \quad (2.4)$$

2.2 SYSTEM SETUP

In most cases, three-dimensional scanning systems rely on one or more optical sources, one or more vision or capturing devices, computer systems, input and output connections, and software to obtain the outside shape structure of the target object. Because extensive hardware and software are required for current 3D scanning systems, one of the most promising developments for the future is the flexibility and portable convenience of a whole system.

Our stereovision system is composed of a pair of 10.2-megapixel Canon® EOS Rebel XTi digital cameras. Each camera is mounted perpendicularly to the ground, and takes the picture for the target from the top. Each camera is set about 13° faced to each other in order to create the convergent angle onto the target. The focal length f is about 28 *mm*, the baseline length b is about 130 *mm*, and the distance from the target to the baseline is about 350 *mm*.

2.3 CAMERA CALIBRATION

Camera calibration denotes the adjusting of internal parameters of each camera according to the position of two cameras. Such internal parameters include two aspects: intrinsic parameters and extrinsic parameters [26, 27]. The first aspect refers to the

distortion happened inside the camera due to the image sensor, and the second aspect results from different positions of left and right cameras.

The ideal calibration pattern design is according to [28], as shown in Figure 2.3, which has two surfaces with the angle of 90 degree. Each surface is full of 9×6 black circles whose diameters are all 7 mm , and the distance between each circle is 15 mm measured from center to center. Through the process of calibration, the circle distortions happening in both cameras can be eliminated, and then the real shape of those 108 circles can be taken on in the result of the scanning system.

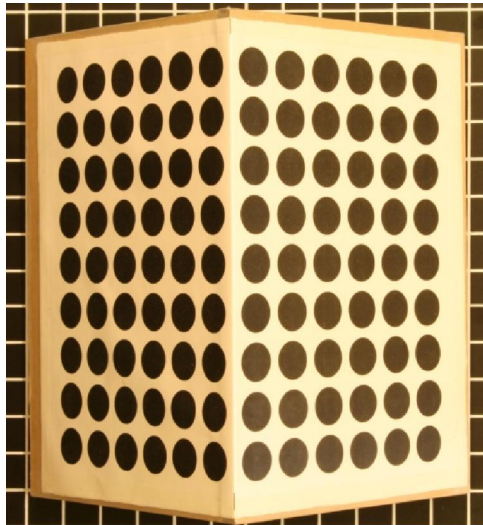


Figure 2.3 System calibration pattern.

Chapter 3: Measurement of Fabric Pilling

3.1 INTRODUCTION

Pilling is a phenomenon that occurs when many clusters of loose fibers are formed on a fabric by repeated abrasions or other mechanic actions in laundering or service. Entangled fiber clusters look like small balls of various sizes floating on the fabric surface. If the fabric surface is flat and levelled, one can simply use a depth threshold to separate pilling areas in the 3D image from the fabric background [15, 29]. However, a fabric is often wrinkled or folded, and the direct depth thresholding may include large surface areas that are not associated with pilling, as shown in Figure 3.1b. The size of a pilling area is also sensitive to the selection of the threshold. Therefore, pilling segmentation should be based on localized depth information rather than a global threshold.

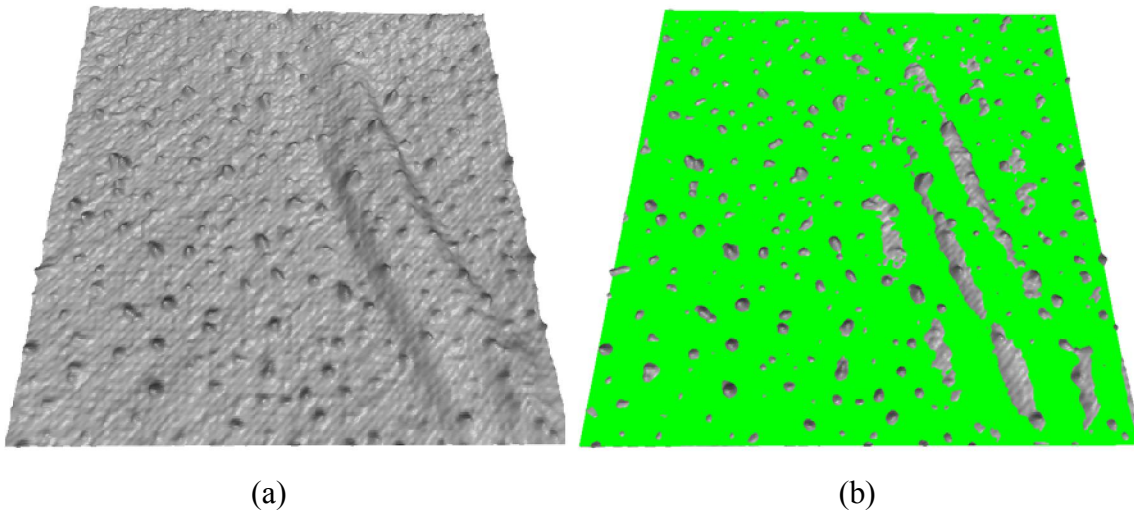


Figure 3.1 Pilling detection result by overall thresholding method, (a) original 3D image and (b) overestimated pilling areas by direct thresholding.

In order to perform a reliable and robust pilling detection method, this chapter will propose a novel algorithm based on local area pilling detection, then, extract feature parameters for pilling evaluation.

3.2 PILLING MEASUREMENT

3.2.1 Pilling Seed Searching

A pill, or a pilling area, has a dune-like shape with one peak (semi-spherical) or two peaks (ellipsoidal), as seen in Figure 3.2. A peak in a mesh region of 3×3 pixels is a point where the height is the maximum relative to its eight-connected neighboring points. A peak can be postulated as a pilling seed— a starting location to search for a possible pill. For an ellipsoidal shape pill (Figure 3.2b), two adjoining peaks will be merged in final pill counting, if the distance between the two peaks is under the given threshold (5 pixels in this project). Figure 3.3a shows the peaks located in Figure 3.1b. Due to the influence of fabric weave structure and noise, these peaks are obviously overestimated, and must be refined to exclude non-pilling peaks.

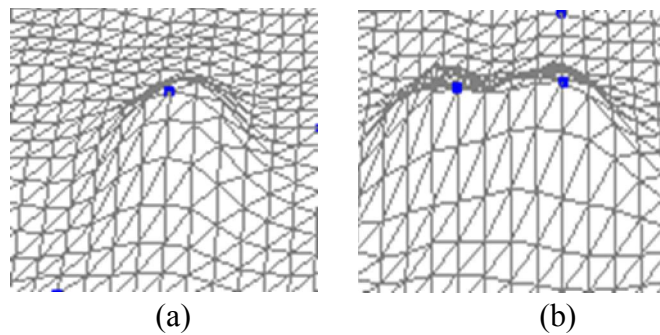


Figure 3.2 Dune-like pills, (a) semi-sphericity shape and (b) ellipsoidal shape.

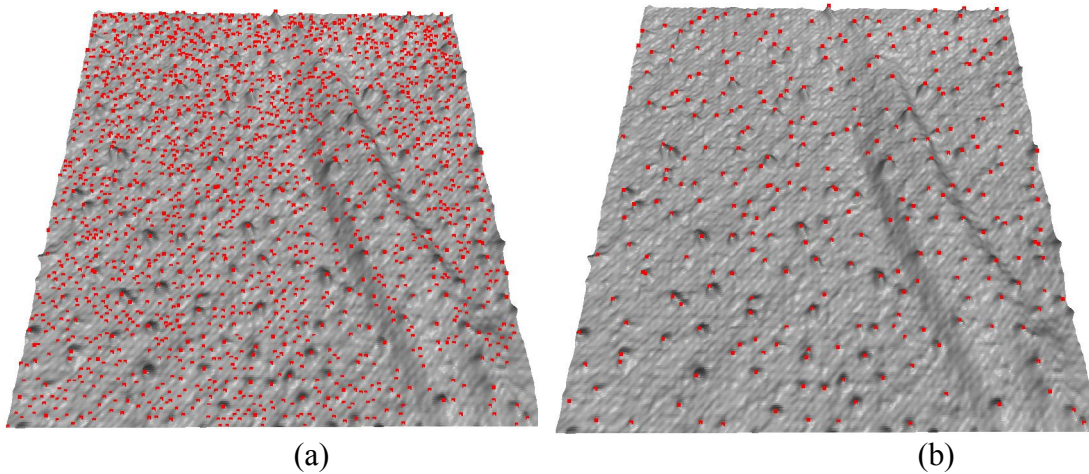


Figure 3.3 Pilling seed detection, (a) peak map and (b) pilling seeds.

The dune-like shape of a pill is the major characteristic that can be used to distinguish a pilling peak from noise or a texture point. For a dune shape, two perpendicular parabolic curves can be found. Generally, a pill's area is around $3 \times 3 \text{ mm}^2$. In the proposed system, according to the yielded resolution, we take a pilling peak as the center of a window (e.g., 10×10 pixels) which will cover most pills sizes. Scan a profile that passes the center horizontally from left to right. If the profile has a parabolic shape, it should move upward to its peak and then downward to the end. Locate the first point where the profile starts the upward trend and the last point where the profile ends the downward trend. If the distance between the two points is larger than the given threshold (5 pixels in this project), register them as the “left” and “right” base points, respectively. The same procedure is applied to the vertical profile to check if the “top” and “bottom” base points exist. If these four base points are found around a peak as seen in Figure 3.4a, the horizontal and vertical profiles are considered parabolic, and such peak is regarded as a candidate for a pilling seed. Otherwise, if one or no pair of base points is found as shown in Figure 3.4b or 3.4c, the peak would be deleted from Figure 3.3a.

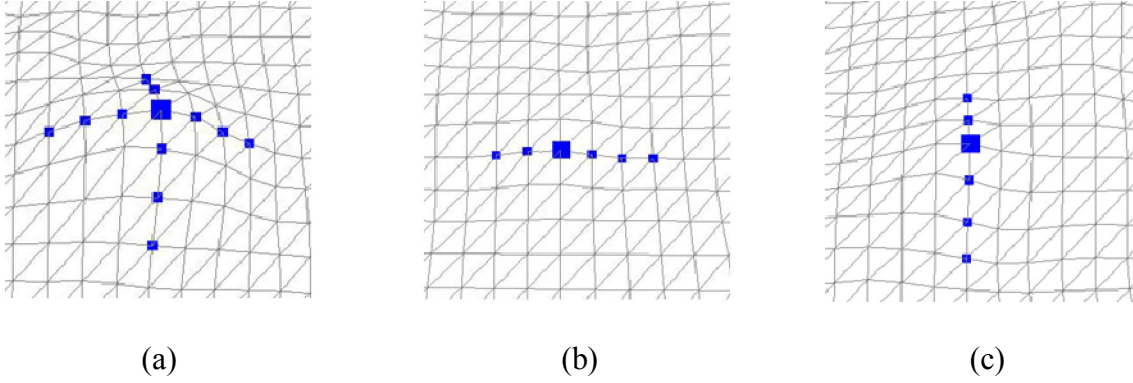


Figure 3.4 Crossing profiles at a peak, (a) dune shape, (b) horizontal profile, and (c) vertical profile.

The four base points can be used to select a base plane for the dune-shaped area, from which the localized peak height can be estimated. The peak height is an important parameter to decide if the peak is finally deemed to be a pilling seed. A plane, expressed in the form of $ax + by + cz = 1$, can be defined by three points. Assume the coordinates of any three base points are (x_1, y_1, z_1) , (x_2, y_2, z_2) , and (x_3, y_3, z_3) . The line coefficients can be calculated as follows:

$$a = \frac{1}{\Delta} \begin{vmatrix} 1 & y_1 & z_1 \\ 1 & y_2 & z_2 \\ 1 & y_3 & z_3 \end{vmatrix}, \quad b = \frac{1}{\Delta} \begin{vmatrix} x_1 & 1 & z_1 \\ x_2 & 1 & z_2 \\ x_3 & 1 & z_3 \end{vmatrix}, \quad \text{and } c = \frac{1}{\Delta} \begin{vmatrix} x_1 & y_1 & 1 \\ x_2 & y_2 & 1 \\ x_3 & y_3 & 1 \end{vmatrix}, \quad (3.1)$$

where Δ is the determinant, i.e., $\Delta = \begin{vmatrix} x_1 & y_1 & z_1 \\ x_2 & y_2 & z_2 \\ x_3 & y_3 & z_3 \end{vmatrix}$. The perpendicular distance from the

forth point (x_4, y_4, z_4) to the plane can be computed when the coefficients are known:

$$Dis = \frac{|ax_4 + by_4 + cz_4 - 1|}{\sqrt{a^2 + b^2 + c^2}} \quad (3.2)$$

With the four points, four different planes can be obtained. The plane with the minimum Dis should be chosen as the base plane for the candidate pill because this plane ensures the minimum difference from the four points. From the base plane, the pill's

height, H , can be calculated. Similar to Dis in equation 3.2, H is the perpendicular distance from the peak point to the base plane when coordinate (x_4, y_4, z_4) is substituted by the peak's coordinate (x_p, y_p, z_p) . In order to make the z_4 more immune to noise, z_p can be replaced by the average z value of its 3×3 neighbouring region:

$$z_p = \underset{n \in N_8(p) \cap p}{mean} [Z(n)], \quad (3.3)$$

where p is the peak position, $N_8(p)$ represents the peak's eight-connected neighbors, and $[Z(n)]$ is the average height in the peak region of 3×3 pixels. A height filter should be used to constrain the minimum peak height because a pill's peak is normally 1 to 3 *mm* above the surface of the fabric. This filter threshold can be estimated by the average of the heights of all four-base points in the image, B_{aver} . Only when a peak passes the pill height filter, it will be labeled as a pilling seed for the region-growing process. The refined pilling seeds from the initial peak map are shown in Figure 3.3b.

3.2.2 Pilling Seed Region Growing

Region growing is a process to expand the pilling area based on a detected pilling seed. Denote all the pilling seeds as C_1, C_2, \dots, C_n , and take a window of 20×20 pixels centered at each seed as the maximum region for seed-growing limitation. A set T represents all as-yet unallocated pixels in the window:

$$T = \{t \notin \bigcup_{i=1}^n C_i \mid N_4(t) \cap \bigcup_{i=1}^n C_i \neq \varnothing\}, \quad (3.4)$$

where $N(t)$ is the set of four-connected neighbours of pixel t . If one of the $N_4(t)$ ($t \in T$) is the neighbour of C_i and $N_4(t) \cap \bigcup_{i=1}^n C_i \neq \varnothing$, the two criteria,

- (1) $\delta(t) = z_{C_i} - z_t$, the depth difference between t and C_i , should be always positive, and
- (2) z_t should be always higher than B_{aver} .

However, because two peaks of an ellipsoidal shaped pill may appear on the pill's top surface, and are within a window of 5×5 pixels centered at C_i , $\delta(t)$ may not be always positive. The current point t only needs to meet $z_t > B_{aver}$, if t is within this window. Beyond the window, point t must qualify both criteria. The process is repeated until no more point meets above requirements in the region of 20×20 pixels. Let S be the set of all detected points in this window and N_s be the number of points in set S . In reality, N_s should be filtered to prevent small noisy regions and large surface features from being counted as pills. In this study, a valid pill size N_s has been set to be in the range of $25 < N_s < 200$ pixels based on many visual examinations. After the procedures have been applied to all seeds $\bigcup_{i=1}^n C_i$, a pilling map (Figure 3.5) will be generated from the 3D fabric image (Figure 3.1a).

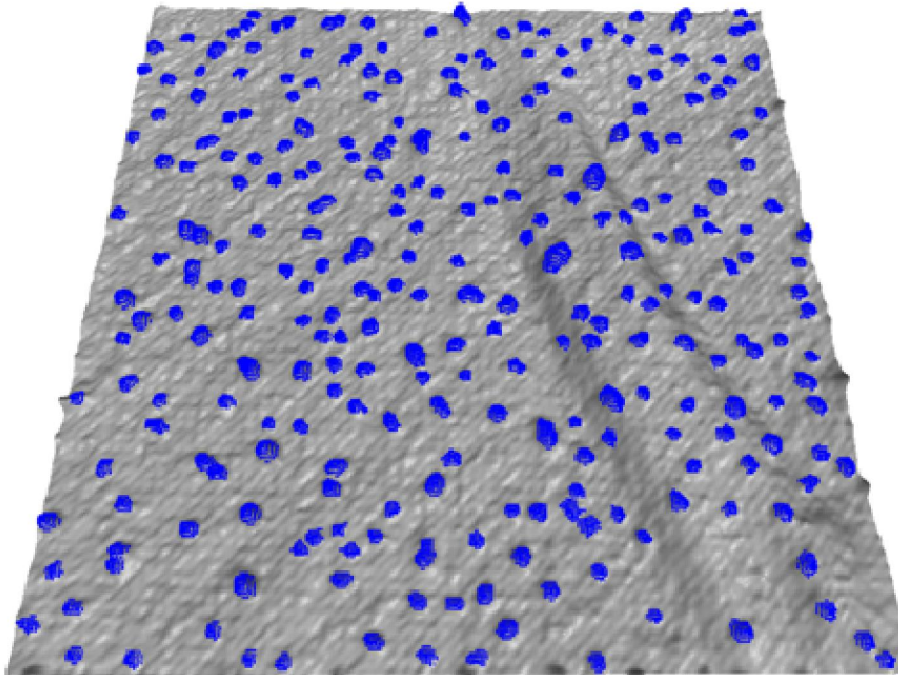


Figure 3.5 Map of detected pilling areas from Figure 3.1a.

3.2.3 Pilling Feature Determination

The severity level of pilling can be evaluated by three important parameters to be extracted after pilling regions are identified: density, height and area of pilling. The density, D , is measured by the count of pilling seeds per a unit area in the image. A pill's height, H , is calculated as the Dis in equation 3.2. A pill's area, A , is considered as the pill's cross-section area on the base plan of the pill. Pixels within a pilling region need to be projected onto the base plane as follows (Figure 3.6):

$$P_p = P_o - N_b \times h, \quad (3.5)$$

where P_o is an original pilling point, P_p is the projected point, $N_b = \frac{1}{\sqrt{a^2 + b^2 + c^2}}(a, b, c)$ is the normal vector of the base plane, and h is the perpendicular distance from P_o to the base plane. In reference to the vertex relation in the 3D mesh, A can be calculated by accumulating the area of each triangle composed by three projected points.

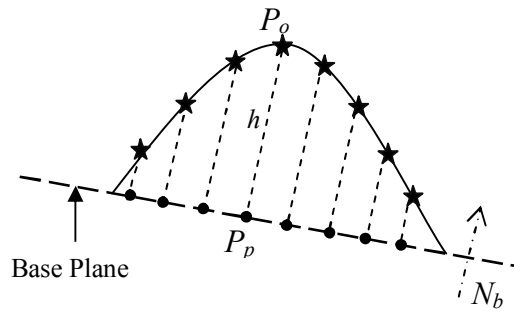


Figure 3.6 Illustration of surface projection onto the base plane.

Chapter 4: Measurement of Fabric Wrinkling

4.1 INTRODUCTION

Former work for 3D wrinkle detection was converting the 3D depth data into a gray scale with 0 to 255 range bitmap image, and then utilizing image processing methods, such as edge detection or wavelet transforming, to find wrinkles on a fabric [29]. These methods showed good results, but the processing method was superfluous. All the procedures were basically 2D image processing, once the wrinkle map was obtained, in order to subtract features of wrinkles, 2D image intensity values should be converted back into depth values again. In this chapter, a new algorithm directly processing 3D depth data will be proposed to detect wrinkling and measure wrinkle features.

4.2 WRINKLE MEASUREMENT

4.2.1 Fabric Surface Leveling

Generally, for local region analyzing, wrinkles always exist with maximum or minimum depth. Maximum points show as ridges in 3D image, while minimum depth points are valleys. Ideally, for a flat fabric, the $z = 0$ plane should be at the center of the fabric thickness. Maximum points should always be above zero to present as ridges, and minimum points are negative to form valleys.

But in practice, fabric samples may have large-scale fluctuation or overall inclination that will produce significant distortion on the 3D surface generated from stereo matching, as seen in Figure 4.1a. It is necessary to remove these large-scale surface variations before locating wrinkle ridges and valleys. The non-uniform rational B-spline (NURBS) surface, as a shape representation commonly used in the geometric

design, can be used to create a surface that best fits in a 3D fabric image. NURBS has two important properties suited for this application. First, it offers a unified mathematical formulation for representing not only free-form surfaces but also standard analytic shapes such as quadrics and sweeping surfaces. Second, by adjusting the positions of control points and manipulating associated weights, it is possible to reconstruct a NURBS surface to represent the basic shape of the surface. These properties make a NURBS surface robust for the approximation of 3D point clouds and remove unwanted elements from the fabric surface [30, 31].

A NURBS surface is defined by its order, a set of weighted control points, and a knot vector $\mathbf{U} = (u_0, \dots, u_k)$ which is a non-decreasing sequence of real numbers, e.g., $u_i \leq u_{i+1}$, $i = 0, \dots, k - 1$. Each u_i is called knots. If we denote the i -th B-spline basis function of degree p by $B_{i,p}(u)$, then a NURBS surface of degree p in the u direction and degree q in the v direction is a vector-valued piece wise rational function $S: [0,1]^2 \rightarrow \mathbf{R}^d$ ($d \in \mathbf{N}$) of the form

$$S(u, v) = \frac{\sum_{i=0}^k \sum_{j=0}^l B_{i,p}(u) B_{j,q}(v) w_{i,j} P_{i,j}}{\sum_{i=0}^k \sum_{j=0}^l B_{i,p}(u) B_{j,q}(v) w_{i,j}}, \quad (4.1)$$

where $P_{i,j}$ are control points in \mathbf{R}^d , and $w_{i,j}$ are the weights of the points $P_{i,j}$. The B-spline basic function $B_{i,p}(u)$ and $B_{j,q}(v)$ are defined on the knot vectors as

$$\mathbf{U} = \left(\underbrace{0, \dots, 0}_{p+1}, u_{p+1}, \dots, u_{r-p-1}, \underbrace{1, \dots, 1}_{p+1} \right), \quad (4.2)$$

and

$$\mathbf{V} = \left(\underbrace{0, \dots, 0}_{q+1}, v_{q+1}, \dots, v_{s-q-1}, \underbrace{1, \dots, 1}_{q+1} \right), \quad (4.3)$$

with \mathbf{U} having $r + 1$ and \mathbf{V} having $s + 1$ knots. It is necessary that $r = k + p + 1$ and $s = l + q + 1$. Setting the rational basic function $R_{i,j}: [0,1]^2 \rightarrow \mathbf{R}^d$ as

$$R_{i,j}(u, v) = \frac{B_{i,p}(u)B_{j,q}(v)w_{i,j}}{\sum_{i=0}^k \sum_{j=0}^l B_{i,p}(u)B_{j,q}(v)w_{i,j}}, \quad (4.4)$$

the surface $S(u, v)$ can be written as

$$S(u, v) = \sum_{i=0}^{k-1} \sum_{j=0}^{l-1} R_{i,j}(u, v)P_{i,j}. \quad (4.5)$$

Therefore, the basic function $R_{i,j}$ are dependent on the weights $w_{i,j}$.

In this application, a fabric surface (\mathbf{R}) constitutes $n \times n$ data points, $(x_i, y_j, z_{i,j})$ for $i, j = 1, \dots, n$. The NURBS approximation is to search for a function that realizes $f(x_i, y_j) \approx z_{i,j}$. This can be done by solving a least-squares problem, resulting in the minimization of the following sum:

$$\sum_{s=0}^n (S(x_s, y_s) - z_s) = \sum_{s=0}^n \left(\sum_{i=0}^k \sum_{j=0}^l R_{i,j}(x_s, y_s) - z_s \right)^2 \quad (4.6)$$

where $R_{i,j}$ is the rational basic function from equation 4.4. Figure 4.1b shows a NURBS surface generated by the approximation using the least-square method. The NURBS surface contains the large-scale (low-frequency) variations of the reconstructed surface. Subtracting Figure 4.1a from Figure 4.1b, one can remove those large-scale components and flatten the fabric surface, while preserving small-scale variations in the differential surface (Figure 4.1c) for wrinkle detection.

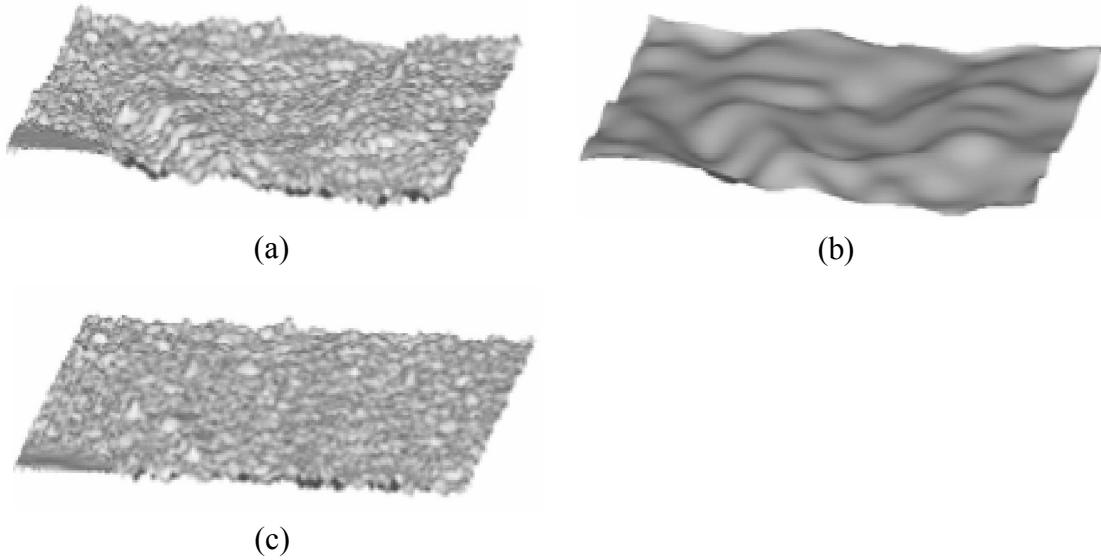


Figure 4.1 3D image surface leveling, (a) raw 3D image data, (b) NURBS surface (elevation plane), and (c) Leveled fabric surface.

4.2.2 Wrinkle Detection

In this project, we defined wrinkle direction according to Figure 4.2. If a wrinkle falls in the range I ($45^\circ \leq \theta < 135^\circ$ and $225^\circ \leq \theta < 315^\circ$), we call this wrinkle a vertical wrinkle, otherwise if it falls in range II, it is a horizontal wrinkle.

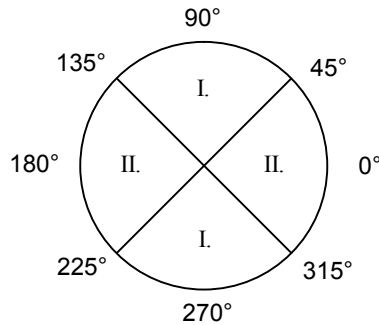


Figure 4.2 Wrinkle direction chart.

After obtaining the leveled fabric surface, we assume the leveled fabric is very close to ideal flat fabric. In other words, on the leveled surface, the wrinkle ridge points should be positive and valley points should be negative. In order to find wrinkle ridge or

valley points, we first narrow the searching range. Ridge happens with an up-trend, once passed over the peak, a down-trend would immediately happen. Valley happens just to the contrary. Thus, the first step is to find the tendency starting point. Because of the leveled fabric, $z = 0$ plane is chosen as the reference plane. We decide if current point $Z_i < 0$ and its next point $Z_{(i+1)} \geq 0$, i is temporally defined as up-trend starting point with mark i_{up} . The down-trend starting point is marked with i_{down} when the current Z_i is above $z = 0$ plane and its next point $Z_{(i+1)} \leq 0$. For vertical wrinkles detection, we follow above rules searching row by row. In each row, we detect all the i_{up} and i_{down} points and store them in the order from left to right. For a wrinkle existing range, the i_{up} and i_{down} should appear in pair, and the distance R_w between i_{up} and i_{down} should not be too short. In this study, we define that the distance R_w should be longer than 3 pixels. If an R_w is determined, within the R_w , an extreme depth point must be found, and such point will be a candidate of wrinkle ridge/valley point. Figure 4.3 shows a close-view of a part of a row in 3D image. Red boxes represent downward tendency starting points, and green boxes are upward tendency starting points. The starting points i_{down_1} and i_{up_1} are stored next to each other which are determined as a pair. The distance R_w between this pair is 8 pixels. Thus, the orange cycled extreme point is cataloged as a valley candidate. Although the starting points i_{down_2} and i_{up_1} , show in a pair, their R_w does not meet our requirements. We just skip searching in this range. Finally, three orange cycled points are found and cataloged as wrinkle candidates in this row.

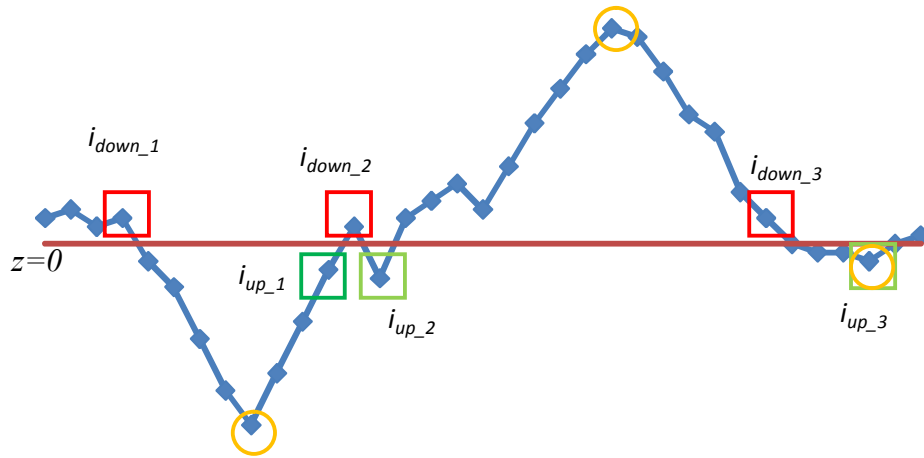


Figure 4.3 Close-view of a part of a row in 3D image.

After all rows are processed, a vertical wrinkle map is produced. The same procedure is applied to each column to detect horizontal wrinkles. An intermediate wrinkle map is created and shown in Figure 4.4b.

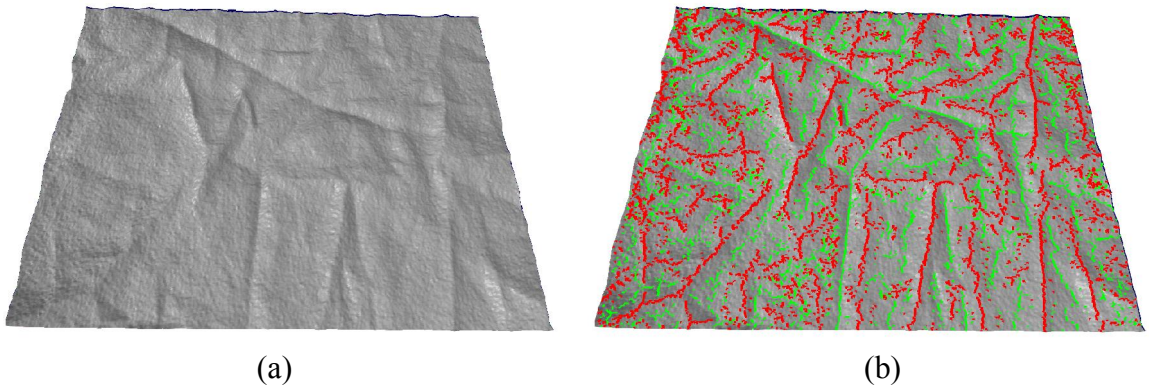


Figure 4.4 Wrinkle detection intermediate result, (a) raw 3D image and (b) intermediate result.

At this time, wrinkles are not continuous, and noises are also detected. Some long wrinkles are broken into several small parts because those broken parts do not meet our preset requirements. In order to make the results closer to human visual detecting

sensation, we manually make up those broken points, and call this procedure linking. For the linking procedure, we first assume that each ruptured wrinkle part is linear, and denote that the connected wrinkle points for each wrinkle consisting of a set W_i .

Here, $W_i = \{(x_1, y_1), (x_2, y_2), \dots, (x_n, y_n)\}$ and W_i should fit a linear line which can be presented as:

$$Y = aX + b \quad (4.7)$$

where $Y = (y_1, y_2, \dots, y_n)$, $X = (x_1, x_2, \dots, x_n)$. Slope a and intercept b can be found according to following equations:

$$a = \frac{(\sum y)(\sum x^2) - (\sum x)(\sum xy)}{n(\sum x^2) - (\sum x)^2} \quad (4.8)$$

$$b = \frac{n(\sum xy) - (\sum x)(\sum y)}{n(\sum x^2) - (\sum x)^2} \quad (4.9)$$

By knowing the linear line, the wrinkle profile direction is determined. Along the wrinkle direction, we manually extend two end points of a wrinkle for 5 pixels. If the extended points meet with other wrinkle points, and such touched wrinkle has a similar direction to the extending wrinkle, we will say these two wrinkle parts can be linked together.

After the linking procedure, a pruning procedure is used to clean the wrinkle map. By analyzing the connected components, all objects which have an area less than n pixels are removed. A minimum object size of $n = 16$ is found to be effective for removing small spurious wrinkles. The final wrinkle map is seen in Figure 4.5.

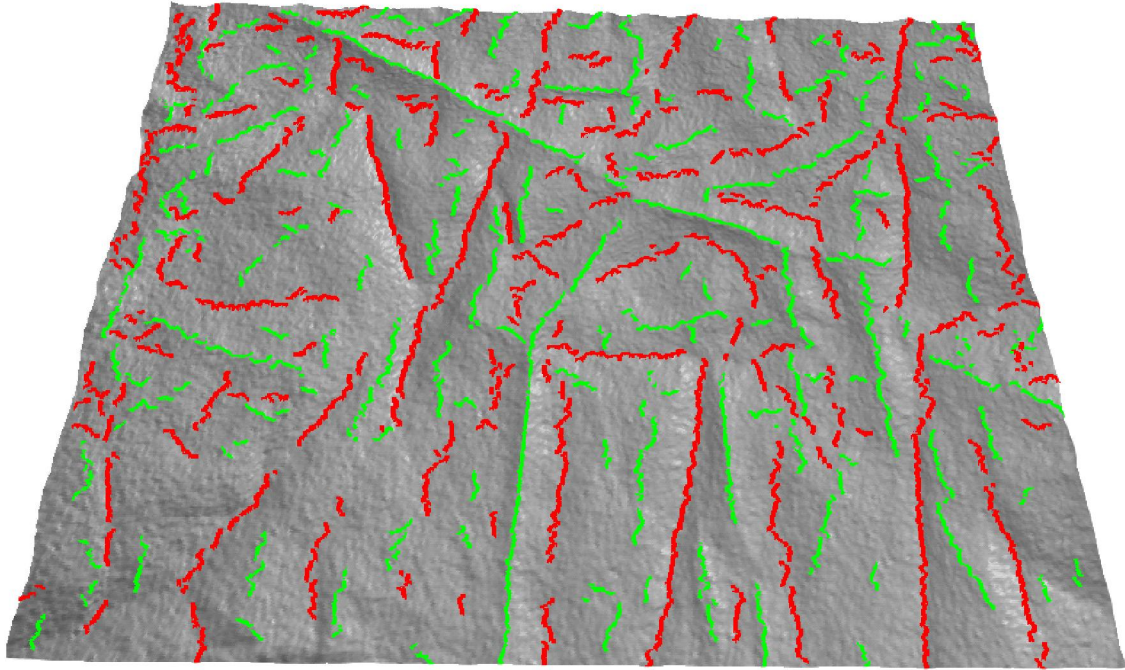


Figure 4.5 Wrinkle detection result.

4.2.3 Wrinkle Feature Extraction

From the 3D wrinkle map, wrinkle geometrical measurements can be performed. Four major parameters including wrinkling density, hardness, tip-angle, and roughness are measured in this study.

Wrinkling density indicates the ratio of total wrinkle length in the sample divided by the sample area.

Wrinkling hardness or sharpness presents the shape of the wrinkle, describing the ratio of the wrinkle height to the width of the wrinkle. Here, the height of the wrinkle is defined as the average ridge or valley height of each wrinkle. The width refers to the distance between two end points of a cross profile which is traced at each ridge or valley pixel by scanning the wrinkle surface transversely (profile *AB* and *CD* in Figure 4.6).

The two endpoints for a cross profile, (x_1, y_1) and (x_2, y_2) for example, should be the two trend starting points (one is up-trend point, another is down-trend point), and they should be fitted on the line $y = -\frac{1}{a}x + (-\frac{1}{a}x_w - y_w)$. Here a is the slope of the wrinkle, which was calculated from equation 4.8. x_w and y_w represent the current wrinkle ridge/valley position.

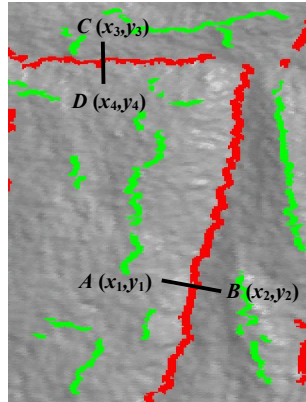


Figure 4.6 Close-up of wrinkle area showing the transverse profile AB and CD .

Wrinkling hardness sometimes may not describe knitted fabrics correctly. For some knitted fabrics, a wrinkle ridge or valley would have a steep angle near the wrinkle top, but when points are near the wrinkle edge, the wrinkle gradient will become slight. Wrinkling tip-angle is introduced to depict the steep angle near the wrinkle ridge or valley.

Wrinkling roughness is described as the variations in wrinkle heights with on consideration of a wrinkle shape. Four parameters are used to define the roughness.

1. Arithmetic average roughness R_a :

$$R_a = \frac{1}{n} \sum |z_{i,j} - p| \quad (4.10)$$

2. Root mean square roughness R_q :

$$R_q = \sqrt{\frac{1}{n} \sum (z_{i,j} - p)^2} \quad (4.11)$$

where $z_{i,j}$ is the height of a wrinkle at position (i, j) , n is the number of total detected wrinkle points, and p is the average height of the scanned surface.

3. Ten-point height R_z describe the average distance between five highest peak z_{pi} and the five lowest valleys z_{vi} on the surface.

$$R_z = \frac{1}{5} \sum_{i=1}^5 (z_{pi} - z_{vi}) \quad (4.12)$$

4. Bearing surface ratio t_p refers to the wrinkle areas above an established reference plane whose height is between the highest peak and the lowest valley to the entire scanned surface area. Such plane intersects the surface and generates a number of subtended surfaces which are above the reference plane.

Chapter 5: Experimental Results Analysis

The purpose of the chapter is to find a data modeling method for the extracted fabric characteristics, which can properly represent the difference in pilling and wrinkling severity levels based on the 3D images generated from stereovision system.

5.1 SAMPLE PREPARATION

5.1.1 Pilling Sample Preparation

The samples used in the experiment were 100% cotton fabrics of different colors and structures that were treated either by random tumbling [32] or home laundering [33]. Each sample was rated on a 5-grade scale by three trained individuals using the ASTM photographic pilling standard [32]. The first grade stands for the worst pilling appearance, the fifth grade represents a non-pilling appearance, and the rest indicate intermediate levels on the scale. From all the visually-rated samples, six samples were picked for each pilling grade. Thus, there were totally 30 samples for comparison tests. The samples were imaged by our stereovision system, and the 3D images were generated and processed using the aforementioned algorithms.

5.1.2 Wrinkle Sample Preparation

3D images generated from 6 wrinkle grading replicas were directly used as training samples. 30 fabrics as testing samples with different fiber contents and weave structures were chosen by an appliance company to validate the evaluation results of the quantitative wrinkle classification method. Each sample was graded with the AATCC SA replicas by the trained personnel. In each level, 5 fabrics were graded.

5.2 PILLING EXPERIMENTS

The first test conducted in the experiment was the repeatability test, in which a sample was imaged three times under the same condition. Table 5.1 displays the 3D images and pilling measurements of the sample in the repeated tests. The three images show no appreciable visual difference. The differences in the measured D , H , and A data are 2.08%, 5.30% and 3.83%, respectively, among the three tests. The difference was calculated by difference between the maximum and the minimum divided by the average of one dataset.

Table 5.1 Illustration of surface projection onto the base plane.

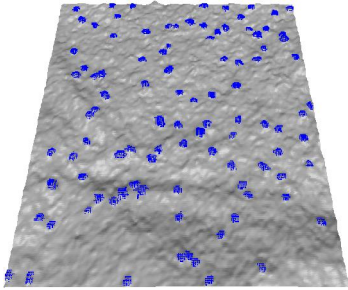
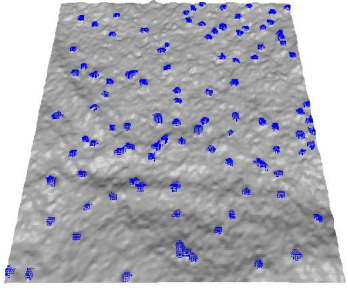
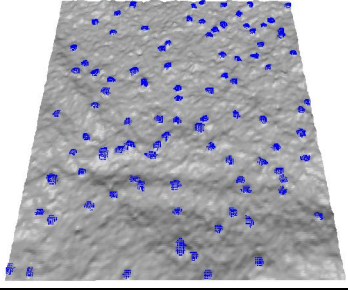
	D (count/cm ²)	H (mm)	A (mm ²)
	2.37	1.25	4.12
	2.42	1.22	4.28
	2.41	1.31	4.14
Difference (%)	2.08	5.30	3.83

Table 5.2 lists the three pilling features measured by the stereovision system and the pilling density counted manually with a special magnifier on the 30 samples. There were five ASTM pilling grades and six samples in each grade in the test. The magnifier for manual counting has a viewing area of $2.5 \times 2.5 \text{ cm}^2$. The comparison between the two methods (3D vs. Manual) could be made only for the pilling densities (D) because the other two pilling measurements (H and A) were difficult to be measured manually. The two sets of D data were compared separately at each grade, and the R^2 (R is the correlation coefficient) ranged from 0.678 at grade 4 to 0.995 at grade 1. When the D s of all the grades were pooled together, the R^2 was 0.985 (see Figure 5.1). In terms of D , the stereovision system gave the highly consistent result with the manual counting.

Table 5.2 3D and manual measurements of pilling density (D), height (H) and area (A).

Grade		Sample		1	2	3	4	5	6	R ²
1	Manual	D (count/cm ²)		4.19	4.50	6.65	4.50	4.19	3.88	0.995
	3D	D (count/cm ²)		4.94	5.34	7.30	5.17	4.86	4.70	
		H (mm)		1.67	0.79	0.79	0.80	0.80	0.80	N/A
		A (mm ²)		9.26	9.60	9.64	9.83	18.53	18.71	N/A
2	Manual	D (count/cm ²)		3.87	2.79	3.10	3.87	3.57	4.03	0.768
	3D	D (count/cm ²)		3.64	2.96	3.49	4.06	3.73	4.58	
		H (mm)		0.79	1.18	0.80	0.50	0.79	0.80	N/A
		A (mm ²)		9.03	12.06	10.34	9.54	8.20	9.71	N/A
3	Manual	D (count/cm ²)		2.17	2.02	2.79	3.10	2.48	2.63	0.682
	3D	D (count/cm ²)		1.96	2.47	2.73	3.21	2.32	2.56	
		H (mm)		0.80	0.80	0.79	0.79	0.80	0.53	N/A
		A (mm ²)		12.12	15.05	8.49	7.92	12.10	11.95	N/A
4	Manual	D (count/cm ²)		0.78	0.78	0.62	0.78	0.93	1.24	0.678
	3D	D (count/cm ²)		0.58	0.57	0.54	0.82	0.63	1.02	
		H (mm)		0.83	0.88	1.27	0.69	0.72	0.82	N/A
		A (mm ²)		4.99	21.67	7.95	7.93	5.05	7.95	N/A
5	Manual	D (count/cm ²)		0	0	0.19	0.23	0	0.08	0.925
	3D	D (count/cm ²)		0.02	0	0.11	0.11	0	0.02	
		H (mm)		0.83	0	0.71	0.79	0	0.79	N/A
		A (mm ²)		7.96	0	5.08	5.25	0	7.45	N/A

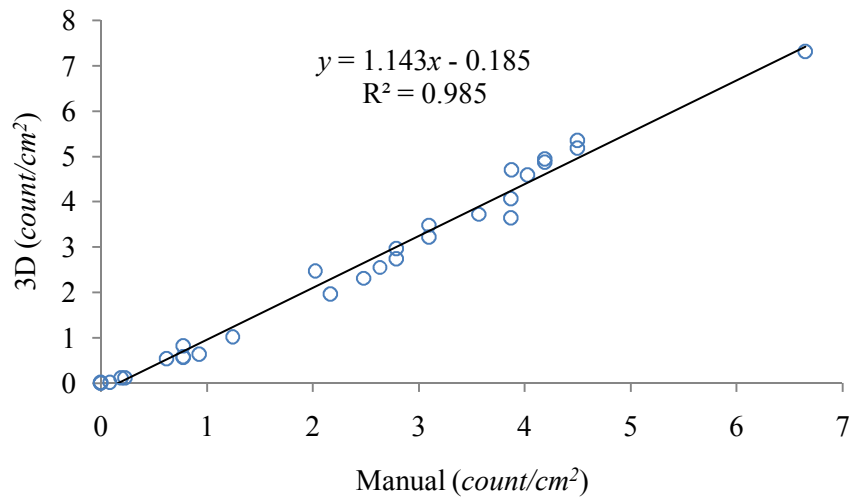


Figure 5.1 Pilling density measurements.

Unlike the pilling density, the pilling height (H) did not change with the pilling grade (G) considerably. For these 30 samples, most of them remained an average H around 0.8 mm, and only three samples had heights above 1 mm. Likewise, the pilling area (A) did not correlate with the G . There was no clear trend that A increased consistently with the severity level of pilling (a smaller G represents more severe pilling). This is because the maximum height and size of a pill in the pilling treatment are dictated by the length of protruding fibers. The latter is influenced mainly by the fiber content, yarn and fabric structures. As the abrading continues, the friction force tends to break fibers and thus produce more fiber clusters. Only fiber ends in the reach of the protruding length can be entangled together. Therefore, the size and height of a pill will not continue to increase with the abrasion. The pilling mechanism in the sample did significantly alter the pilling counts. This was also evidenced by the multivariate regression analysis in Table 5.3 for the three parameters (D , H , and A) obtained from 3D images of the 30 samples. The pilling grade (G) had a high correlation with the D ($R^2 = 0.923$), and was

improved slightly by including the A and H in the equations. Thus, the pilling grade estimation can be based on a sole measurement— D . However, pilling height and area are still useful information for assessing severity of pilling, especially among fabrics with different fiber contents and structures.

Table 5.3 Regression analysis between pilling grades and pilling features.

Model	R ²	Equation
D	0.923	$G = -0.674D + 4.673$
D and A	0.938	$G = -0.632D - 0.043A + 4.977$
D, A and H	0.942	$G = -0.624D - 0.035A - 0.376H + 5.175$

The pilling grade classification can be also performed by using traditional classifiers. Three classifiers including the logistic regression [34], the naïve Bayes classifier [34], and the linear support vector machines (SVM) [35] were applied. For each of the 30 samples, four 3D images were generated from different regions. The total 120 images were divided into three subsets, S_1 , S_2 , and S_3 , by selecting eight images for each of five grades. Of the three subsets, two were used for the training test, and the third for the validation test. The cross-validation test was repeated three times for each of the three classifiers. Tables 5.4, 5.5, and 5.6 list the classification results and accuracies of the three classifiers. The accuracy was evaluated by the ratio of the predicted grade over the corresponding visual grade. In these tables, each column represents the visual grades, and each row gives the predicted grades from the classifiers. At grades 4 and 5, the accuracies for all the three classifiers appeared to be lower than at the other grades in the cross-validation tests. This might be due to the fact that the poor photographic quality of grades 4 and 5 in the ASTM standard affected visual judgements for the samples whose pilling appearance fell in this range. However, the logistic regression classifier had the classification accuracies of three subsets above 0.775, and its average accuracy was the

highest among the three classifiers, and thus was chosen to be the pilling classifier for the future test.

Table 5.4 Classification by the logistic regression classifier.

		Visual Grade														
		S_1					S_2					S_3				
		1	2	3	4	5	1	2	3	4	5	1	2	3	4	5
Predicted Grade	1	8	0	0	0	0	7	1	0	0	0	8	1	0	0	0
	2	0	7	1	0	0	1	6	1	0	0	0	7	1	0	0
	3	0	1	6	1	0	0	1	7	0	0	0	0	6	2	0
	4	0	0	1	5	1	0	0	0	6	3	0	0	1	5	2
	5	0	0	0	2	7	0	0	0	2	5	0	0	0	1	6
Accuracy		1.00	0.88	0.75	0.63	0.88	0.88	0.75	0.88	0.75	0.63	1.00	0.88	0.75	0.63	0.75
Overall		0.825					0.775					0.80				
Average accuracy of three subsets												0.80				

Table 5.5 Classification by the naïve Bayes classifier.

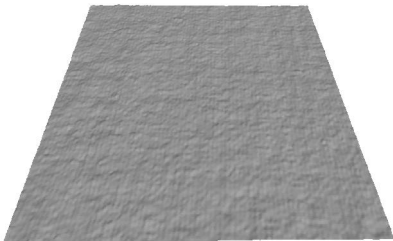
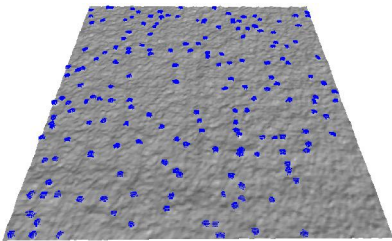
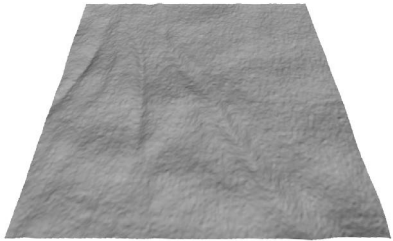
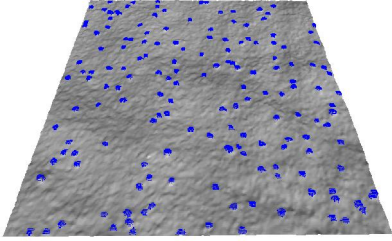
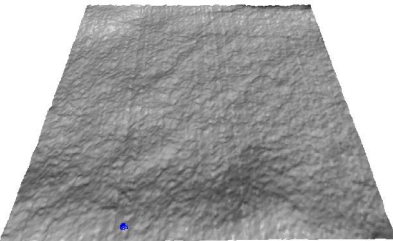
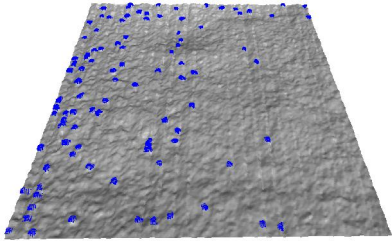
		Visual Grade														
		S_1					S_2					S_3				
		1	2	3	4	5	1	2	3	4	5	1	2	3	4	5
Predicted Grade	1	5	1	0	0	0	4	1	0	0	0	4	1	0	0	0
	2	3	6	1	0	0	4	5	2	0	0	4	7	2	0	0
	3	0	1	7	0	0	0	2	6	2	0	0	0	6	3	0
	4	0	0	0	5	4	0	0	0	5	3	0	0	0	4	3
	5	0	0	0	3	4	0	0	0	1	5	0	0	0	1	5
Accuracy		0.63	0.75	0.88	0.63	0.50	0.50	0.63	0.75	0.63	0.63	0.50	0.88	0.75	0.5	0.63
Overall		0.675					0.625					0.65				
Average accuracy of three subsets												0.65				

Table 5.6 Classification by the linear SVM.

		Visual Grade														
		S_1					S_2					S_3				
		1	2	3	4	5	1	2	3	4	5	1	2	3	4	5
Predicted Grade	1	6	2	0	0	0	6	1	0	0	0	7	1	0	0	0
	2	2	5	2	0	0	2	5	3	0	0	1	6	2	0	0
	3	0	1	6	2	0	0	2	5	2	0	0	1	6	2	0
	4	0	0	0	5	2	0	0	0	5	2	0	0	0	6	3
	5	0	0	0	1	6	0	0	0	1	6	0	0	0	0	5
Accuracy		0.75	0.63	0.75	0.63	0.75	0.75	0.63	0.63	0.63	0.75	0.88	0.75	0.75	0.75	0.63
Overall		0.70					0.675					0.75				
Average accuracy of three subsets												0.708				

The stereovision can be used to visually and quantitatively trace appearance changes of samples due to home laundering. Table 5.7 displays the 3D images and the pilling densities of three different samples before and after being treated in 25 laundering cycles. Samples 1 and 2 were solid color fabrics, and sample 3 was a fabric with a striped color pattern. Before the treatment of 25 laundering cycles, the three samples appeared to have no or little pilling. After the 25 washed cycles, the pilling became obvious on the surface of these samples with the pilling density varying from 2 to 4 pills/cm². The 3D measured results matched with the manual detected results, which the R² values for both original and treated samples were close to 1.

Table 5.7 3D images and pilling densities of three different samples.

	Original	Density (count/cm ²)		Treated	Density (count/cm ²)	
		3D	Manual		3D	Manual
1		3D	0.00		3D	3.97
		Manual	0.00		Manual	4.13
2		3D	0.00		3D	3.68
		Manual	0.00		Manual	3.83
3		3D	0.02		3D	2.01
		Manual	0.03		Manual	2.15

5.3 WRINKLE EXPERIMENTS

Six 3D wrinkle replica images corresponding to AATCC 124 six grades [13] were the training samples. The four major features, wrinkling density, sharpness, tip-angle, and roughness made a 4-dimensional feature vector. However, wrinkle roughness was described by four parameters, which would expand the feature vector into 8 dimensions. It seems that measurement accuracy will decrease when we place 4 subset parameters as the same level as 4 major defects, and redundant calculation will happen as well. We try to reduce four wrinkle roughness parameters to less than four or even one component. In other words, the four-dimensional wrinkle roughness vector will be reduced into fewer dimensions. In order to transform a higher-dimensionality feature vector to a smaller-dimensionality vector, feature extraction algorithms are used to interpret the raw feature vectors. Principal-component analysis (PCA) is one of the feature extraction algorithms, which uses an orthogonal transformation to convert a set of correlated variables into a set of values of linearly uncorrelated variables. PCA finds the best “subspace” that captures as much data variance as possible. In this study, we used PCA to do wrinkle roughness dimension reduction processing. Before applying PCA, the raw wrinkle roughness listed in Table 5.8 should be converted into normalized data by z-score, which is uniform to different scaled data and improves comparability. The z-score normalization is based on equation 5.1, and the normalized data are shown in Table 5.9.

$$Normalized(n_i) = \frac{n_i - \bar{N}}{std(N)} \quad (5.1)$$

where

$$\bar{N} = \frac{1}{n} \sum_{i=1}^n n_i \quad n = 6 \quad (5.2)$$

$$std(N) = \sqrt{\frac{1}{(n-1)} \sum_{i=1}^n (n_i - \bar{N})^2} \quad (5.3)$$

Table 5.8 Wrinkle roughness raw data.

Grade	R_a	R_q	R_z	t_p
1	0.126	0.158	0.701	0.499
2	0.090	0.112	0.441	0.499
3	0.060	0.076	0.307	0.038
3.5	0.053	0.067	0.258	0.033
4	0.052	0.066	0.286	0.026
5	0	0	0	0

Table 5.9 Normalized wrinkle roughness data.

Grade	R_a	R_q	R_z	t_p
1	1.4818	1.4831	1.5976	1.2892
2	0.6283	0.6103	0.4714	1.2892
3	-0.0830	-0.0727	-0.1090	-0.5886
3.5	-0.2489	-0.2435	-0.3213	-0.6089
4	-0.2726	-0.2625	-0.2000	-0.6375
5	-1.5055	-1.5147	-1.4388	-0.7434

Based on the data listed in Table 5.9, according to Table 5.10 (the importance of components analyzed by PCA), the number of reduced dimensions can be determined.

Table 5.10 Importance of components.

	Component 1	Component 2	Component 3	Component 4
Standard deviation	1.7684	0.4482	0.0727	0.0004
Proportion of variance	93.81%	6%	0.1%	0.09%
Cumulative proportion	93.8%	99.84%	99.99%	100%

From Table 5.10, the proportion of variance row shows that component 1 occupies the most proportion which is close to 95%. This result indicates that one dimension will be sufficient to represent four wrinkle roughness parameters, which means the four-dimensional wrinkling roughness feature vector will be reduced to one dimension. The PCA dimensional reduction results plotted in Figure 5.2 demonstrates, generally speaking, the better separability for the given classes.

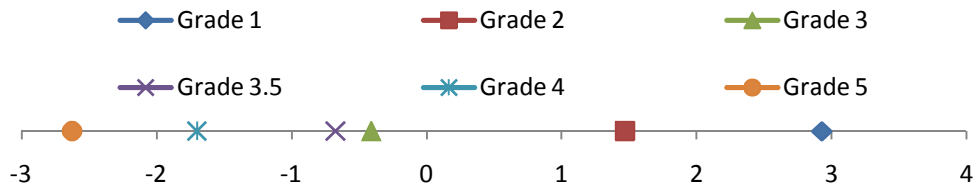


Figure 5.2 Distribution of one dimensional wrinkle roughness feature vector by PCA.

Similar to pilling classification procedure, each of 30 wrinkle fabrics generated six 3D images from each fabric different regions. The total of 180 3D wrinkling images was randomly divided into three subsets, S_1 , S_2 , and S_3 . The cross-validation was performed. Because the logistic regression classifier was used for pilling classification, we still chose it for wrinkling classification. Table 5.11 lists the 180 images cataloged

results and the result accuracy of the logistic regression classifier. For the wrinkle severity of level 1, 2, 4, and 5, all levels showed a good accuracy in which values were above 70%. The worst accuracy happened between level 3 and level 3.5 which has the accuracies around 60%. This makes sense because, even though samples in these two levels are graded by visual method, we still may not tell to which grades these samples belong. But the overall accuracy for the logistic regression classifier is acceptable at 74.4%.

Table 5.11 The logistic regression classification results of 180 3D wrinkling images.

		Visual Grade																	
		S_1						S_2						S_3					
		1	2	3	3.5	4	5	1	2	3	3.5	4	5	1	2	3	3.5	4	5
Predicted Grade	1	9	0	0	0	0	0	8	1	0	0	0	0	8	1	0	0	0	0
	2	1	8	1	0	0	0	2	8	1	0	0	0	2	7	1	0	0	0
	3	0	1	6	2	1	0	0	1	5	2	0	0	0	2	6	3	0	0
	3.5	0	1	3	7	1	0	0	0	4	7	1	0	0	0	2	6	1	0
	4	0	0	0	1	7	2	0	0	0	1	8	1	0	0	1	1	8	1
	5	0	0	0	0	1	8	0	0	0	0	1	9	0	0	0	0	1	9
Accuracy		0.9	0.8	0.6	0.7	0.7	0.8	0.8	0.8	0.5	0.7	0.8	0.9	0.8	0.7	0.6	0.6	0.8	0.9
Overall		0.750						0.750						0.733					
Average accuracy of three subsets		0.744																	

Chapter 6: Conclusions and Future Work

6.1 SUMMARY OF THE THESIS

An integrated fabric wrinkling and pilling appearance evaluation system based on 3D stereovision technique was presented in this study. Comparing with 2D image processing, 3D imaging technology has the advantage in measuring fabric surface and shape, which fully utilizes the depth information while disregarding fabric texture, color, and intensity information that may be varied by different light sources. After reviewing current laser or other light sources based on 3D surface imaging systems, the proposed stereovision system provide a portable, affordable, efficient and high resolution 3D imaging system.

A stereovision system that only needs a pair of consumer grade high resolution cameras and mounting hardware to support two cameras in parallel is more cost effective than other 3D imaging systems with laser or structured lights source requirements. Image acquisition time that is less than 10 micro seconds presents the higher efficiency for the proposed system. The system only needs to be calibrated when the relative positions of the cameras are changed. A portable calibration target was designed for the stereovision system. These properties contribute to the portability of the system and also reduce the cost of maintenance.

By taking advantage of data with the depth information obtained from stereovision system, two major fabric appearance features, pilling and wrinkling, were detected and measured. A novel pilling detection algorithm based on 3D imaging local information was proposed. Pilling density, height, and size were extracted features for pilling severity classification. A fast wrinkle detection algorithm with leveled 3D surface showed a good wrinkle detection result. Four measurands including wrinkling density,

sharpness, tip-angle, and roughness were measured, and they would be the basis of wrinkle level classification. Both measurements for pilling and wrinkle were repeatable. Comparing with the time consuming visual rating method, the proposed 3D fabric surface measurement showed a better efficiency and more objectiveness.

The pilling densities measured from the 3D images of 30 samples were highly correlated with those counted manually ($R^2 = 0.985$). Although only the pilling density consistently changed with the pilling grade for the given set of samples, the pilling height and area should be useful parameters for assessing pilling appearance, especially for fabrics with different fiber contents and structures.

120 3D pilling images were used to find a suitable classifier based on three quantitated pilling features. The logistic regression classifier performed the best result with 80% in comparison with the naïve Bayes classifier and the linear SVM. We also chose the logistic regression classifier for wrinkling severity classification. 180 3D wrinkling images gathered from 30 wrinkling-severity-determined fabrics were used to evaluate the chosen classifier validity based on the four wrinkling features. The overall accuracy for wrinkle grading was 74.4%. The poorest classifications happened on wrinkle level 3 and level 3.5 whose accuracies were around 60%. Because level 3.5 was added to describe a smooth, non-pressed fabric appearance, the boundary of level 3.5 and 3 are not easy to be distinguished, even when judged by the visual method.

6.2 SUGGESTED FUTURE WORK

There is still room to improve the pilling and wrinkle detection algorithm. Pilling detection for some thicker thread fabrics is easy to overestimate because those thread connection parts will be misunderstood as small pills by a computer. Recently, the system

only allows manually adjusting pilling detecting parameters. More studies relating to fabric of different fibers need to be done in the future.

More pilling and wrinkle samples need to be tested to verify the validity of the logistic regression classifier and the repeatability of the proposed pilling and wrinkle detection algorithm. The major difference between wrinkle level 3 and 3.5 should be the tip-angle. Level 3.5 describes smoother wrinkling in fabrics with small tip-angles in comparison with level 3. In the future, with sufficient wrinkle samples, the fabric wrinkle tip-angle may be considered to apply more weight when processing the classification.

Bibliography

- [1] B. Xu and J. A. Reed, "Instrumental evaluation of fabric wrinkle recovery," *Journal of The Textile Institute*, vol. 86, pp. 129-135, 1995.
- [2] Y. Na and B. Pourdeyhimi, "Assessing wrinkling using image analysis and replicate standards," *Textile Research Journal*, vol. 65, pp. 149-157, 1995.
- [3] R. Zaouali, S. Msahli, B. El Abed, and F. Sakli, "Objective evaluation of multidirectional fabric wrinkling using image analysis," *Journal of The Textile Institute*, vol. 98, pp. 443-451, 2007.
- [4] C. J. Choi, H. J. Kim, Y. C. Jin, and H. S. Kim, "Objective wrinkle evaluation system of fabrics based on 2D FFT," *Fibers and Polymers*, vol. 10, pp. 260-265, 2009.
- [5] B. Xu, "Instrumental evaluation of fabric pilling," *Journal of the Textile Institute. Part 1, Fibre science and textile technology*, vol. 88, pp. 488-500, 1997.
- [6] Y. Torres, and R. Navarro, "Automatic method based on image analysis for pilling evaluation in fabrics," *Optical Engineering*, vol. 37, pp. 2937-2947, 1998.
- [7] J. R. Wagner, "Development of an image analysis algorithm for assessing pilling," *Nonwovens Coference*, pp. 305-312, 1999.
- [8] B. Xin, J. Hu, and H. Yan, "Objective evaluation of fabric pilling using image analysis techniques," *Textile Research Journal*, vol. 72, pp. 1057-1064, 2002.

- [9] S. Jingjing, Y. Ming, X. Bugao, and P. Bel, "Fabric wrinkle characterization and classification using modified wavelet coefficients and support-vector-machine classifiers," *Textile Research Journal*, vol. 81, pp. 902-913, 2011.
- [10] M. Yao, W. Yu, W. Xu, and B. Xu, "Evaluating fabric fuzziness using laser range sensing," *Optical Engineering*, vol. 47, pp. 013603-013603, 2008.
- [11] T. J. Kang, D. H. Cho, and H. S. Whang, "A new objective method of measuring fabric wrinkles using a 3-D projecting grid technique," *Textile Research Journal*, vol. 69, pp. 261-268, 1999.
- [12] J. Su and B. Xu, "Fabric wrinkle evaluation using laser triangulation and neural network classifier," *Optical Engineering*, vol. 38, pp. 1688-1693, 1999.
- [13] AATCC Test Method 124, "Technical manual of the American Association of Textile Chemists and Colorists," *AATCC*, Research Triangle Park, NC, 2003.
- [14] A. E. Johnson, "Can Wrinkle-Prone Fabrics Be Identified?," *Am. Dyest. Rep.*, vol. 58, pp. 13-15, 1969.
- [15] B. Xu, W. Yu, and R. Wang, "Stereovision for three-dimensional measurements of fabric pilling," *Textile Research Journal*, vol. 81, pp. 2168-2179, 2011.
- [16] W. Yu and B. Xu, "A sub-pixel stereo matching algorithm and its applications in fabric imaging," *Machine Vision and Applications*, vol. 20, pp. 261-270, 2009.
- [17] B. Xu, D. F. Cuminato, and N. M. Keyes, "Evaluating fabric smoothness appearance with a laser profilometer," *Textile Research Journal*, vol. 68, pp. 900-906, 1998.

- [18] N. Abidi, E. Hequet, C. Turner, and H. Sari-Sarraf, "Objective evaluation of durable press treatments and fabric smoothness ratings," *Textile Research Journal*, vol. 75, pp. 19-29, 2005.
- [19] M. Z. Brown, D. Burschka, and G. D. Hager, "Advances in computational stereo," *Pattern Analysis and Machine Intelligence, IEEE Transactions on*, vol. 25, pp. 993-1008, 2003.
- [20] R. Zabih and J. Woodfill, "Non-parametric local transforms for computing visual correspondence," in *Computer Vision—ECCV'94*, Springer, 1994, pp. 151-158.
- [21] B. K. Horn and B. G. Schunck, "Determining optical flow," *Artificial intelligence*, vol. 17, pp. 185-203, 1981.
- [22] V. Venkateswar and R. Chellappa, "Hierarchical stereo and motion correspondence using feature groupings," *International Journal of Computer Vision*, vol. 15, pp. 245-269, 1995.
- [23] C. E. Leiserson, R. L. Rivest, and C. Stein, *Introduction to algorithms*, Ed. T. H. Cormen, The MIT press, 2001.
- [24] C. Tomasi and R. Manduchi, "Stereo matching as a nearest-neighbor problem," *Pattern Analysis and Machine Intelligence, IEEE Transactions on*, vol. 20, pp. 333-340, 1998.
- [25] Y. Boykov and V. Kolmogorov, "An experimental comparison of min-cut/max-flow algorithms for energy minimization in vision," *Pattern Analysis and Machine Intelligence, IEEE Transactions on*, vol. 26, pp. 1124-1137, 2004.

- [26] J. Heikkila and O. Silven, "A four-step camera calibration procedure with implicit image correction," in *Computer Vision and Pattern Recognition, 1997 IEEE Computer Society Conference on*, pp. 1106-1112, 1997.
- [27] R. Y. Tsai, "A versatile camera calibration technique for high-accuracy 3D machine vision metrology using off-the-shelf TV cameras and lenses," *Robotics and Automation, IEEE Journal of*, vol. 3, pp. 323-344, 1987.
- [28] Z. Zhengyou, "A flexible new technique for camera calibration," *Pattern Analysis and Machine Intelligence, IEEE Transactions on*, vol. 22, pp. 1330-1334, 2000.
- [29] Y. Ming, "Fabric wrinkle and pilling evaluation by stereovision and three dimensional surface characterization," *Master Thesis, University of Texas at Austin*, 2012.
- [30] B. F. Gregorski, B. Hamann, and K. I. Joy, "Reconstruction of B-spline surfaces from scattered data points," in *Computer Graphics International*, pp. 163-170, 2000.
- [31] G. Gunther and H. Kai, "Interpolating and Approximating Scattered 3D-data with Hierarchical Tensor Product B-Splines," In *Proceedings of Chamonix*, pp. 1, 1996.
- [32] ASTM Standard D3512, "Random tumble pilling test method," *ASTM International*, West Conshohocken, PA, DOI: 10.1520/D3512_D3512M-10E02, 1999.

- [33] AATCC Test Method 143, "Appearance of apparel and other textile end products after repeated home laundering," *AATCC*, Research Triangle Park, NC, 2011.
- [34] T. M. Mitchell, M. Generative, and D. Classifiers, "Naïve Bayes and logistic regression," *Machine learning*, vol. 10, p. 701, 2005.
- [35] C. Cortes and V. Vapnik, "Support-vector networks," *Machine learning*, vol. 20, pp. 273-297, 1995.